

# Performance Limits of a Micromachined Tunable-Cavity Filter

Jung-sik Moon and Andrei M. Shkel

Microsystems Laboratory, Department of Mechanical and Aerospace Engineering  
University of California, Irvine, CA 92697, USA

jmoon@uci.edu, ashkel@uci.edu, [html://mems.eng.uci.edu](http://mems.eng.uci.edu)

## ABSTRACT

This paper focuses on the performance limits of a tunable-cavity Fabry-Perot filter (FPF) implemented using MEMS technology. This is a versatile device capable of many functions, including light modulation and high precision sensing. Our goal is to explore challenges and opportunities in implementing tunable-cavity filter using MEMS technology. Thermal stability and effects of fabrication imperfections are studied. Based on coupled-field modeling analysis, it is concluded that the device is extremely sensitive to thermal fluctuations and fabrication imperfections degrading performance significantly. It is emphasized that if these challenges are appropriately addressed, the device will be a low cost alternative to existing DWDM filters and variety of precision sensors.

**Keywords:** Fabry-Perot Interferometer, Etalon, Surface Micromachining, Multiphysics modeling, MEMS

## 1 INTRODUCTION

Classical wavelength interferometers are a collection of hand assembled etalons, which consist of two semi-transparent mirrors separated by a fixed-cavity. Individual etalons are designed with a different cavity size, each responsible for filtering a specific wavelength. Commonly used in telescopes and optical measurement devices, tunable filters are in high demand in telecommunication industry, where the goal is to filter wavelengths from  $1550nm$  to  $1630nm$ , crucial for Dense Wavelength Division Multiplexing (DWDM). However, a single etalon costs approximately \$300, making a wide tunable filter assembly costly.

A possible alternative to this discrete approach is the implementation of wide band tunable filter using MEMS technology, in a single device. This approach will allow a single tunable device to replace an array of fixed-cavity filters. MEMS technology offers many advantages, including scalability for wide tuning range, sensitivity for precision sensing, and batch fabrication capability for cost reduction. However, MEMS technology introduces many new challenges, such as fabrication yield, device reproducibility, and fabrication imperfections, all are factors limiting performance. Although

high sensitivity may be beneficial for precision sensors, it is equally disadvantageous due to sensitivity to undesirable perturbations. Considering all advantages and disadvantages, it is critical to understand how limitations inherent to MEMS technology affect performance of a micromachined tunable-cavity filter.

A tunable-cavity Fabry-Perot filter is the focus of this paper, though several other approaches are possible, e.g., diffraction grating, rotating etalon, and “linear sliding” filter, Fig. 1. While exploring available methods suitable for micromachining technology, wide tuning capability, low polarization, and reduced processing steps made tunable-cavity FPF most attractive.

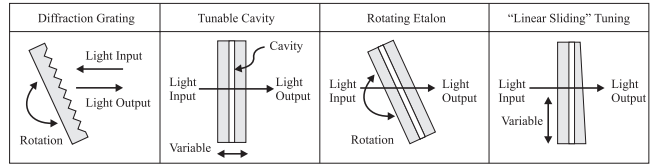


Figure 1: Four tuning methods for interferometry

## 2 FABRY-PEROT PRINCIPLE

A Fabry-Perot filter (FPF) is a device that transmits a selected wavelength or frequency by interference of multiple beams through a reflective cavity formed by two flat, partially transmitting, parallel mirrors separated by a medium, Fig. 2.

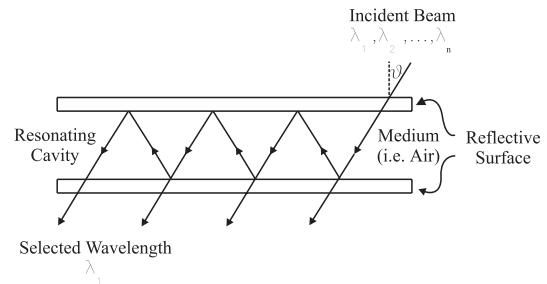


Figure 2: Fabry-Perot filter schematic

Incident light enters the Fabry-Perot cavity, and undergoes multiple reflections, where individual wavelengths

interfere constructively (wavelengths in phase) or destructively (wavelengths out of phase). The constructive wavelength resonates, and this condition is satisfied when the following expression holds [1]:

$$nd \cos \theta = \frac{m\lambda}{2} \quad (1)$$

Here  $\theta$  is the incident light angle normal to the mirror,  $\lambda$  is wavelength,  $d$  is the cavity length,  $n$  is the refractive index of the medium, and  $m$  is an arbitrary integer. For normal incident light, with air as the medium ( $n = 1$ ), the resonating cavity equals multiples of a half wavelength. Resonating light is analogous to a mechanical system operating on the resonance principle. When the resonance conditions are met, a selected portion of the light spectrum resonates and escapes the Fabry-Perot cavity. An important equation describing the intensity ( $T$ ) of the transmitted wavelength for an ideal FPF is given by the Airy function [1]:

$$T = \left(1 - \frac{A}{(1-R)}\right)^2 \frac{1}{1 + \frac{4R \sin^2(kd \cos(\theta - \frac{\pi}{2}))}{(1-R)^2}} \quad (2)$$

where  $A$  is mirror absorptance,  $T$  is mirror transmittance,  $R$  is mirror reflectance, and  $k$  equals to  $2\pi/\lambda$ .

From examination of Eq. (2), intensity is influenced by cavity gap, incident beam angle, and the refractive index. By taking advantage of these parameters, high precision sensing or light modulating applications are realized.

## 2.1 Finesse

Finesse is a figure of merit for defining the performance of a Fabry-Perot filter, determining the number of channels or fringes it can transmit effectively. A high finesse value results in sharper transmission peaks and narrow bandwidth, increasing the resolution and allowing additional channels for greater data density. Therefore, understanding factors affecting finesse of the filter is crucial in defining the performance limits.

Wavelength between consecutive interference fringes is the free spectral range ( $FSR_R$ ) given by

$$FSR_R = \frac{\lambda^2}{2dn}, \quad (3)$$

and full width of the transmittance curve at half of the maximum intensity is the full width half maximum ( $FWHM$ ) given by

$$FWHM_R = \frac{\lambda(1-R)}{n\pi\sqrt{R}}, \quad (4)$$

then reflectance finesse ( $F_R$ ) is defined as the ratio of the free spectral range over the full width half maximum [1]:

$$F_R = \frac{FSR_R}{FWHM_R} = \frac{\pi\sqrt{R}}{(1-R)} \quad (5)$$

Notice  $F_E$  only depends on the reflectance. Fig. 3 is an illustration of an interferometer's transmission profile with definitions, which describe performance.

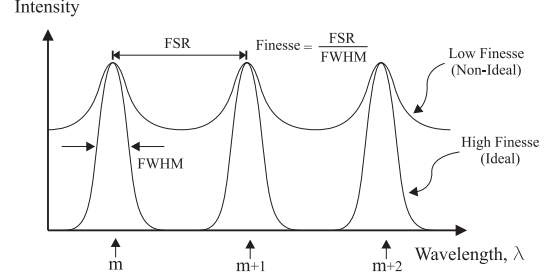


Figure 3: Interferometer's transmission profile and notions defining device performance

## 3 METHODOLOGY

In practice, effective finesse ( $F_E$ ) of a Fabry-Perot filter is measured empirically, and reflectance finesse is calculated from (5). Using these results, the defect finesse ( $F_D$ ) is deduced from the following equation [3]:

$$\frac{1}{F_E^2} = \frac{1}{F_R^2} + \frac{1}{F_D^2} \quad (6)$$

A good survey for calculation of effective finesse is given by Palik in [2]. A real Fabry-Perot filter's performance is limited by the mirror's imperfections, which include reflectance, non-parallelism, and mirror aberrations. One common approach for modeling these defects is based on projecting all surface defects to one reflective surface, considering the other mirror perfectly flat, and convoluting the surface aberrations and the Airy function, Eq. (2). This technique assumes that the non-ideal mirror is a collection of infinitesimal perfectly parallel mirrors with variable cavity lengths, and the integration over elemental mirrors results in the transmission profile of the non-ideal surface [3]. An illustration of the convolution of surface defects can be seen in Fig. 4.

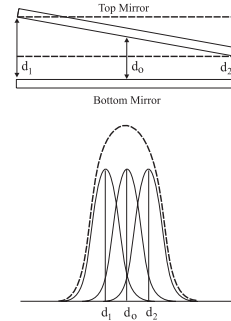


Figure 4: Parallelism error model (adopted from [3])

Illustration of this technique is given by Atherton in [4], where three distinct types of defects are presented.

Based on this work, defect finesse due to departure from parallelism, spherically bowed plates, and surface irregularities is given by:

$$F_p = \frac{\lambda}{3^{\frac{1}{2}}\delta_p}, F_s = \frac{\lambda}{2\delta_s}, F_{rms} = \frac{\lambda}{4.7\delta_{rms}}$$

where  $\delta_p$  and  $\delta_s$  are the parallel and spherical deviations from a planar reference, and  $\delta_{rms}$  is the root-mean-square deviation following a Gaussian distribution. Representing all three defects simultaneously yields [5]:

$$F_D = \left[ \frac{1}{F_p^2} + \frac{1}{F_s^2} + \frac{1}{F_{rms}^2} \right]^{-\frac{1}{2}} = \frac{\lambda}{(3\delta_p^2 + 4\delta_s^2 + 22\delta_{rms}^2)^{\frac{1}{2}}} \quad (7)$$

Once  $F_D$  is known,  $F_E$  is calculated by substituting Eq. (7) into Eq. (6). Generally, a good approximation of  $F_E$  is made with the assumption that imperfect mirrors have defects which are Lorentzian, and  $F_D > F_R$ . Analogous to Eq. (5), the notion of effective reflectance  $R_E$  is given by

$$F_E = \frac{\pi\sqrt{R_E}}{1 - R_E} \quad (8)$$

Further, the transmission function  $T(\lambda)$  of an imperfect etalon can be written as

$$T(\lambda) = T_{pk} \left[ \frac{(1 - R_E)^2}{1 + R_E^2 - 2R_E \cos(2\pi m)} \right] \quad (9)$$

where the transmission peak  $T_{pk}$  is

$$T_{pk} = \left( 1 - \frac{A}{1 - R} \right)^2 \left( \frac{1 - R}{1 + R} \right) \left( \frac{1 + R_E}{1 - R_E} \right)$$

## 4 PERFORMANCE LIMITS

Using results described in Section 3, a relationship between mirror imperfections and effective finesse is developed. In particular, defects arising as a result of mask misregistration and thermal expansion are modeled. Results of modeling are projected to parallel deviations from a planar surface, and then used to solve for effective finesse (Eq. (8)) and the transmission (Eq. (9)). Although, in a real system, all imperfections are present simultaneously, the models serve as an illustration for performance limitations caused by common problems related to MEMS technology.

### 4.1 Coupled-Field Modeling

ANSYS Multiphysics finite element modeling package was used to solve for the coupled electrostatic/structural system response using the command macro ESSOLV. The solid model of the device included a  $100 \times 100\mu m$  mirror suspended by four beams ( $8\mu m$  wide,  $2\mu m$  thick,

$60\mu m$  long) on four corners and a  $100 \times 100\mu m$  electrode placed under the suspended mirror, separated by an air filled  $2\mu m$  optical cavity. Thermal expansion modeling was done by applying a temperature load on all areas with load steps from  $258.15K$  to  $358.15K$ , in  $20K$  increments. Material properties used in simulation were as follows: Young Modulus =  $1.7 \times 10^5 [MPa]$ , Poisson's ratio = 0.3, free space permittivity =  $8.85 \times 10^{-6} [pF/\mu m]$ , electrical permittivity of air =  $1 [pF/\mu m]$ , and coefficient of thermal expansion =  $2.3 \times 10^{-6} [1/K]$ .

### 4.2 Misregistration

Modeling for a tunable-cavity Fabry-Perot filter with expected mask or wafer assembly misregistration was performed. Simulation was done by offsetting the electrodes from  $1\mu m$  to  $4\mu m$  along one of the plane axis, in increments of  $1\mu m$ . For each offset parameter, the mirror was actuated by applying  $0V$  to  $38V$ , causing vertical and angular mirror deflection due to uneven electrostatic pressure. When  $0.5\mu m$  vertical deflection was reached for different offset parameters, angular deflection of 2.5, 3.8, 6.1, and  $8.8 \times 10^{-3}$  degrees were calculated, that corresponded to  $1\mu m$ ,  $2\mu m$ ,  $3\mu m$ , and  $4\mu m$  electrode offset. Fig. 5 is a plot of effective finesse as a function of reflectance for misregistrations  $1\mu m$  ( $A_1$ ),  $2\mu m$  ( $A_2$ ),  $3\mu m$  ( $A_3$ ), and  $4\mu m$  ( $A_4$ ).

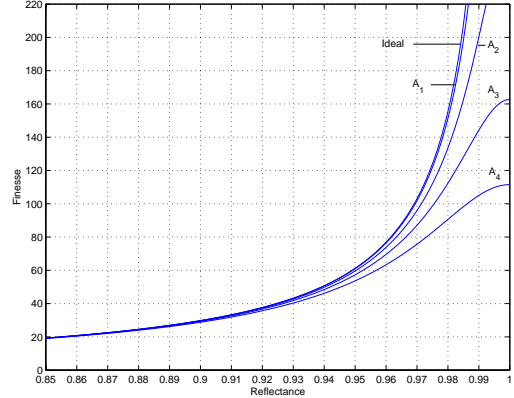


Figure 5: Effective finesse influenced by misregistration

Although the non-parallelism defect is not critical when reflectance is between 85% to 93%, finesse dependence becomes much more pronounced as reflectance increases. For instance, effective finesse of an ideal FPF is 61 and 155 for reflectance values of 95% and 98%, but with  $4\mu m$  mask misregistration causing  $8.8 \times 10^{-3}$  degrees tilt (curve ( $A_4$ ) in Fig. 5), the effective finesse reduces to 55 and 90, respectively. This indicates that defects are the limiting factor as reflectance approaches 100%. A complementing transmission profile for all misregistration at 98% reflectance is plotted in Fig. 6. As misregistration increases, fringe broadening effect becomes more apparent.

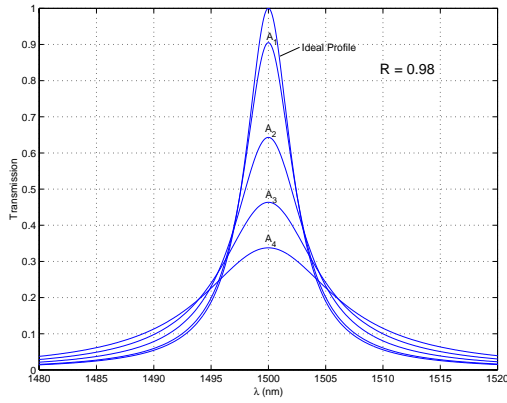


Figure 6: Fringe broadening due to non-parallelism

### 4.3 Thermal Expansion

Operational temperature requirement for Fabry-Perot filters is between  $-20^{\circ}C$  and  $80^{\circ}C$  ( $258.15K$  to  $358.15K$ ). From thermal expansion modeling results, mirror vertical deflection of  $-15.6$ ,  $-7.8$ ,  $0$ ,  $7.8$ ,  $15.6$ , and  $23.3nm$  were calculated, corresponding to  $258.15K$  ( $B_1$ ),  $278.15K$  ( $B_2$ ),  $298.15K$  ( $B_3$ ),  $313.15K$  ( $B_4$ ),  $333.15K$  ( $B_5$ ), and  $358.15K$  ( $B_6$ ). Similar to the non-parallel mirror case, cavity gap fluctuates with temperature, broadening bandwidth and reducing finesse. Although temperature fluctuation is not a mirror defect, conceptually one can visualize the thermal expansion as an instantaneous plate deflection. Therefore, thermal expansion of the mirror can be represented as a non-parallel plate defect. For simplification,  $-15.6nm$  at  $258.15K$  ( $B_1$ ) is treated as the reference position. Using reflectance of 95% and 98% as in the previous example,  $100K$  increase ( $B_6$ ) decreases effective finesse by approximately 33% and 66%, respectively. Fringe broadening effects caused by temperature fluctuations are plotted in Fig. 7. Initially at 98% reflectance, an ideal Fabry-Perot filter's ( $B_1$ ) bandwidth (full width half maximum) equals  $15nm$ . However at  $358.15K$  ( $B_6$ ) bandwidth increases to approximately  $30nm$ , reducing finesse by a factor of two.

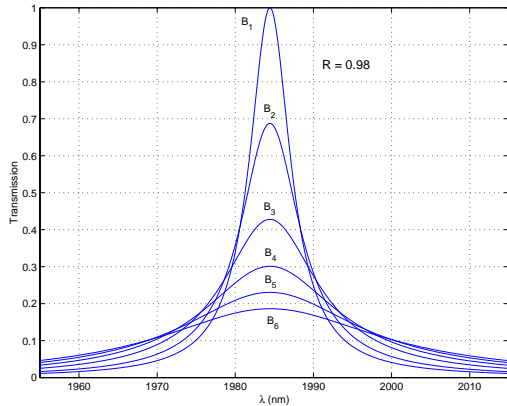


Figure 7: Fringe broadening due to thermal expansion

## 5 CONCLUSION

The paper studied the potential for implementing a high performance tunable-cavity interferometer. It was concluded, based on thermal expansion and component misregistration analysis, that a passive Fabry-Perot filter cannot achieve performance required for DWDM applications. For this application, in order to transmit 40 channels, finesse must be equal to approximately 1000, where spacing of 100 GHz (0.8 nm) and bandwidth up to 10 GHz (0.08 nm) are needed. By depositing gold or silver, reflective materials typically used in optical MEMS applications, 95% reflectance can be achieved. At this reflectance, finesse for an ideal Fabry Perot filter is approximately 61. However, finesse is further aggravated by  $4\mu m$  misregistration, resulting in mirror tilt on the order of 0.01 degrees, reducing effective finesse by as much as 10%. Using the same 40 channels example, reflectance must be higher than 99.69% to be useful for DWDM applications. Current MEMS technology does not satisfy these requirements. However, if multiple dielectric coatings are applied, desirable reflection can be achieved. The use of dielectric coatings requires additional fabrication steps and introduces residual stress that induces mirror curvature. Furthermore, if the defect finesse is greater than the reflectance finesse, there is no benefit in applying a high reflectance coating. This tradeoff between development of new fabrication technology and potential for active compensation of imperfections will be the future focus of this research group.

## REFERENCES

- [1] J. Jerman, D. Clift, and S. Mallinson, "Minature Fabry-Perot Interferometer with a Corrugated Silicon Diaphragm Support," *Sensors and Actuators A (Physical)*, 29(2):151-8, November 1991.
- [2] E. Palik, H. Boukari, and R. Gammon, "Experimental study of the effect of surface defects on the finesse and contrast of a Fabry-Perot interferometer," *Applied Optics*, 35(1):38-50, January 1996.
- [3] C. Roychoudhuri and M. Hercher, "Stable multi-pass Fabry-Perot interferometer: design and analysis," *Optical Engineering*, 20(6):806-14, November-December 1981.
- [4] P. Atherton, N. Reay, J. Ring, and T. Hicks, "Tunable Fabry-Perot Filters," *Applied Optics*, 16(9):2514-20, September 1977.
- [5] J. McKay, "Single and tandem Fabry-Perot etalons as solar background filters for lidar," *Applied Optics*, 38(27):5851-57, September 1999.